IEEE Photonics Journal
An IEEE Photonics Society Publication

Open Access

Mid-Infrared, Ultra-Broadband, Low-Loss, Compact Arbitrary Power Splitter Based on Adiabatic Mode Evolution

Volume 11, Number 2, April 2019

Jia Xu Brian Sia
Wanjun Wang
Xin Guo
Jin Zhou
Zecen Zhang
Mohamed Said Rouifed
Xiang Li
Zhong Liang Qiao
Chong Yang Liu
Callum Littlejohns
Graham T. Reed
Hong Wang

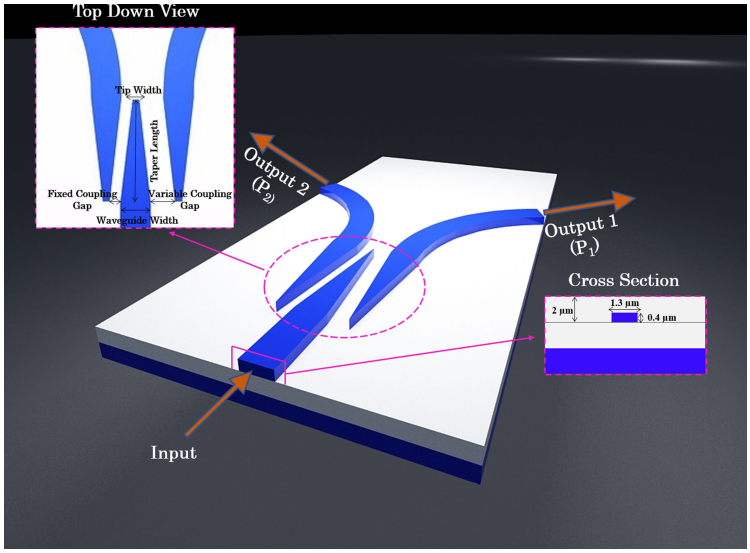

DOI: 10.1109/JPHOT.2019.2907788
1943-0655

Mid-Infrared, Ultra-Broadband, Low-Loss, Compact Arbitrary Power Splitter Based on Adiabatic Mode Evolution

Jia Xu Brian Sia,[1] Wanjun Wang,[1] Xin Guo,[1] Jin Zhou,[1] Zecen Zhang,[1] Mohamed Said Rouifed,[1] Xiang Li,[1] Zhong Liang Qiao,[1] Chong Yang Liu,[1] Callum Littlejohns,[1,2] Graham T. Reed,[1,2] and Hong Wang [1]

[1]Novitas, Silicon Centre of Excellence, School of Electrical and Electronic Engineering, Nanyang Technological University, 639798 Singapore
[2]Optoelectronics Research Centre, University of Southampton, Southampton SO17 1BJ, U.K.

DOI:10.1109/JPHOT.2019.2907788

Manuscript received January 30, 2019; revised March 13, 2019; accepted March 23, 2019. Date of current version April 11, 2019. This work was supported in part by the National Research Foundation Singapore under Grant NRF-CRP12-2013-04, and in part by the Nanyang Technological University-A*Start Silicon Technologies Centre of Excellence. Corresponding author: H. Wang (e-mail: ewanghong@ntu.edu.sg).

Abstract: We designed and demonstrated TE-mode arbitrary power splitters based on adiabatic mode evolution. The power splitters are designed with a footprint of smaller than 12 $\times$ 2.9 μm^2, fabricated on a 400-nm silicon-on-insulator platform, requiring only a single etch step. The optimization process and the conditions for arbitrary-power splitting are performed using three-dimensional-FDTD simulations. We prove this concept through the fabrication of asymmetrical adiabatic evolution-based power splitters with splitting ratios of 50:50, 60:40, and 70:30. The fabricated devices are shown to agree closely with simulation results. Broadband operation with low insertion loss of 0.11–0.6 dB is demonstrated across the 3.66–3.89 μm wavelength range (230 nm). This component has applications in a multitude of areas such as spectroscopic optical sensing and optical phased arrays photonic integrated circuits etc.

Index Terms: Waveguides, mid infrared, photonic integrated circuits, silicon photonics.

1. Introduction

Silicon photonics stands to be a highly desirable platform for the scalable implementation of photonic applications due it its fabrication compatibility with mature CMOS technologies [1], [2], and thus enabling low cost manufacturing of Photonic Integrated Circuits (PIC) at high volume. Interest in Mid-Infrared (MIR) Photonics has been gaining momentum in both academia and industry. This is due to several reasons: with the exponential upturn in communication traffic, leading to an imminent "capacity crunch" [3], there is a pressing need to explore potential options to avoid this "crunch". The 2 μm band is being touted as a potential candidate to alleviate the communication traffic bandwidth problem by enabling long-haul optical communications [4]. The use of the MIR band is not limited to communications; some potential applications include on-chip fusion of IR sensor signals, waveguide amplifiers, radars, and lab-on-chip integrated sensors [5]. With the recent developments in health

monitoring, the automotive industry and medicine, comprehensive and precise data gathering, and analysis techniques are highly desired. Current data gathering techniques utilize the UV band, which is detrimental to human health. The MIR band provides an attractive alternative to the current state of art; many gases have significant absorption lines in the MIR band [6]; examples include CO ($\sim$4.5 μm), CO_2 (2.65 μm, 4.2–4.3 μm), CH_4 (3.2–3.45 μm), and $CH_2O, HCl, HBr, C_6H_{12}O_6$ (3.68–3.88 μm) [7], [8]. Moreover, it has been indicated that silicon waveguides can potentially enable low loss transmission up to 8.5 μm [9], [10]. To date, various MIR devices such as low-loss waveguides [11], tunable laser [12], [13], modulator [14], [15], photodetector [16], sensor [17], have been demonstrated on the silicon photonics platform [18]–[20].

Broadband arbitrary power splitters with low insertion loss are imperative for the realization of high density PICs. Circuit designers can exploit broadband power splitting devices for the realization of high-fidelity multi-channel circuits, enabling parallel processing, leading to gains in operational efficiency. Instances of such PICs include Optical Phased Arrays (OPA) [21] and On-Chip Sensing Circuits. With regards to optical sensing, input light will be split into 2 paths. One path will be used for sensing while the other will be used as a reference; subtracting environmental noise from the experimental results. In recent years, there have been numerous demonstration of power splitters. Other than the standard MMI design, arbitrary power splitting has been achieved through modifications in the multimode region [22–25]. Directional Couplers [26], [27] can also attain the above functionality via the physics of rib waveguide dispersion or asymmetric-waveguide based phase control. The listed examples are however not exhaustive. Interferometric and evanescent coupling-based devices tend to suffer from wavelength selectivity. Narrow bandwidth appears to be an implicit feature of the abovementioned approaches. Of all the design schemes proposed in the literature, Adiabatic Taper-based power splitters [28–30] seems to provide the most promising performance in terms of insertion loss, bandwidth, fabrication complexity and footprint.

By making use of adiabatic mode evolution, we demonstrate low loss, broadband, compact arbitrary power splitters at the 3.8 μm spectral band by fabricating asymmetrically spaced tapers on the 400 nm silicon-on-insulator (SOI) platform (Fig. 1). Lumerical 3D-FDTD simulation indicates arbitrary power splitting with an operation bandwidth of larger than 230 nm across the 3.8 μm waveband. We prove this concept by fabricating splitters with ratios of 50:50, 60:40 and 70:30. To the best of our knowledge, the arbitrary power splitters demonstrate low insertion loss (0.11–0.6 dB) across the largest operation bandwidth of 230 nm (limited by the tunable range of our laser) in silicon photonics. On-Chip Spectroscopic sensing circuits at the 3.8 μm waveband can be implemented with the proposed broadband devices as a key component.

2. Device Design

In this work, we experimentally demonstrate broadband, low loss, arbitrary power splitters based on the adiabatic mode evolution on the 400 nm SOI platform. To ensure that only the fundamental TE mode is supported in the strip waveguide, simulations were performed using the Finite Difference Eigenmode Solver; the width of the single mode strip waveguide is designated to be 1.3 μm. Fig. 1 depicts the three-dimensional schematic of the proposed TE-mode arbitrary power splitter. A fundamental TE-mode input strip waveguide is tapered down and inserted into 2 output tapers with the same length. With regards to the input TE-mode, it will be squeezed out as it travels along the input taper since it will not be supported as the taper width reduces from w_1 to w_2. By varying the coupling gap on one side of the taper, arbitrary splitting ratios can be achieved. As shown in the Fig. 2a, the travelling mode will be enhanced and concentrated in the gaps between the tapered waveguides due to electric field discontinuities. Following, the lossless eigenmodes will be coupled into the two inverse output tapers. The mode evolution process along the length of the taper is shown in Fig. 2b; the top view of the proposed power splitter is shown in Fig. 2c.

To obtain low loss and large bandwidth adiabatic mode evolution, it is imperative to ensure that only the fundamental TE-mode is excited along the length of the taper. A 3D-FDTD simulation of the 3-dB coupler (symmetrical gap) was first carried out to determine the optimal taper length at wavelength of 3.8 μm. The coupling gaps (Variable and Fixed Coupling Gap) and tip width are

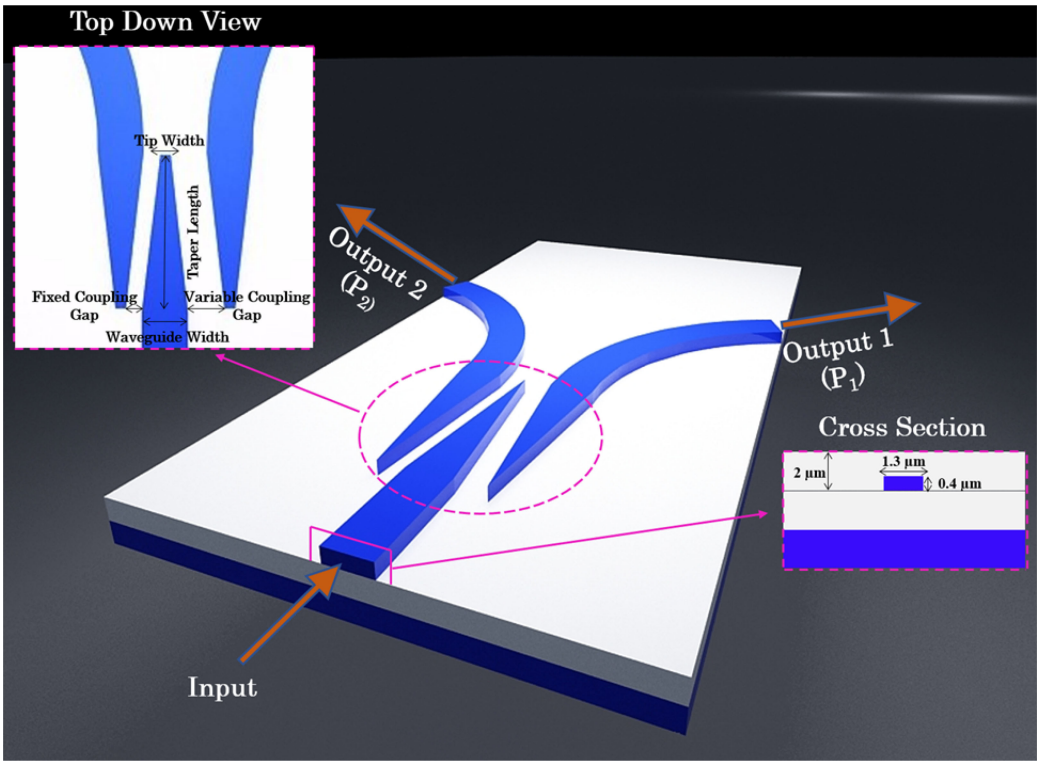

Fig. 1. 3D schematic of proposed power splitter.

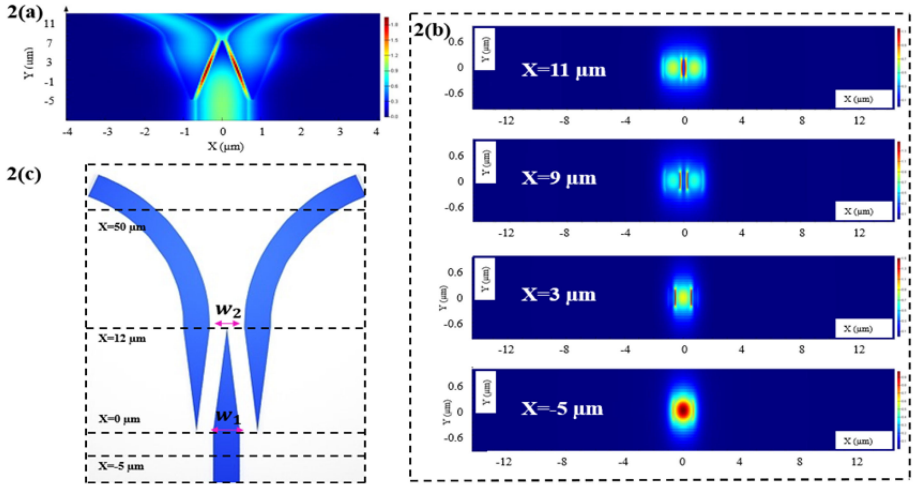

Fig. 2. (a) Electric field distribution of TE mode along the device. (b) Cross-sectional view of mode evolution along the taper length. (c) Top view of proposed device; the coordinates in the direction of light propagation.

initially assumed to be 100 nm and 60 nm, respectively. From Fig. 3(a), we can see that when the taper length exceeds 12 μm, the simulated insertion loss becomes almost negligible. To examine the effect that tip width and coupling gaps have on simulated insertion loss and bandwidth, we performed a 3D-FDTD simulation on a 3-dB coupler with a taper length of 12 μm. When the tip width is varied from 30 to 120 nm with both coupling gaps fixed at 100 nm, according to Fig. 3(b),

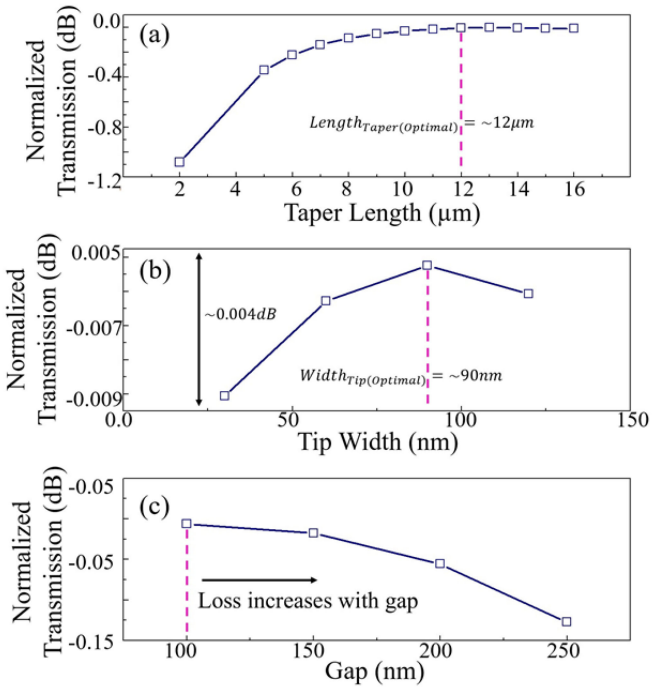

Fig. 3. (a) Variation of simulated insertion loss against taper length. (b) Variation of simulated insertion loss against tip width. (c) Variation of simulated insertion loss against gap for the 3-dB coupler.

the optimal tip width is shown to be 90 nm. However, gains in efficacy is shown to be extremely marginal when tip widths are varied from 30 to 120 nm. Device performance has a high degree of tolerance to tip width, which is extremely important for repeatability between devices. Following, we examine the optimal gap for the 3-dB coupler. From Fig. 3(c), when the gap is decreased from 250 to 100 nm, the simulated insertion loss decreases. We did not consider gaps smaller than 100 nm to ensure compatibility with commercial CMOS process lines.

Following the above design optimization, the taper length, coupling gaps and tip width are selected to be 12 μm, 100 nm and 100 nm respectively. We performed mode analysis (Eigenmode Solver) at the positions x = 2, 4, 6, 8, 10 μm along the length of the coupling region and found that higher mode excitation only occurs from x = 10 μm onwards. The TE00 and TE01 modes at positions x = 10, 10.5, 11, 11.5 μm (Fig. 2c) are shown in Fig. 4(a)–4(h). The effective refractive indices of TE00 and TE01 at the abovementioned taper positions are computed in Fig. 4(i). Indicated in Fig. 4(j), as light propagates along the length of the taper, from positions x = 10 to 12 μm, the difference between the effective refractive index of TE00 and TE01 decreases. This implies that coupling loss from TE00 to TE01 becomes easier as light propagation approaches the end of the taper. However, as TE01 is not supported throughout the entire coupling region, higher order modes are expected to be better suppressed.

Fig. 5(a) shows that arbitrary power splitting can be achieved by increasing the variable coupling gap on one side of the power splitter. However, when the variable coupling gap is increased, the simulated insertion loss increases. The effective refractive index analysis was carried out for arbitrary spitting ratios (60:40, 70:30, 80:20, 90:10). As the splitting ratio is varied from 60:40 to 90:10, the difference between the effective refractive index of TE00 and TE01 decreases (Fig. 5(b)). Coupling loss from TE00 to TE01 becomes more viable. It is however likely that coupling loss from TE00 to TE01 does not represent the main source of device insertion loss. Rather, as Wang. *et al.* [24] have stated, TE polarization is sensitive to sidewall roughness during the mode transition process in the coupling region. Simulation indicates that all arbitrary splitting ratios have a bandwidth

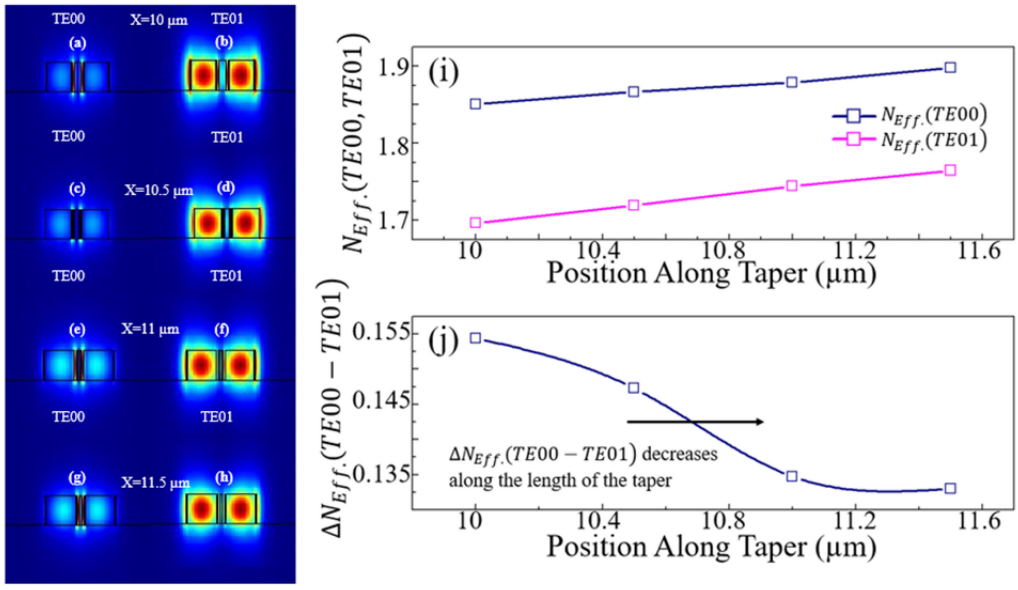

Fig. 4. (a)–(h) Cross section of TE00 and TE01 modes along the length of the taper. (i) Effective refractive index of TE00 and TE01 along the length of the taper. (j) Difference in effective refractive index along the length of the taper.

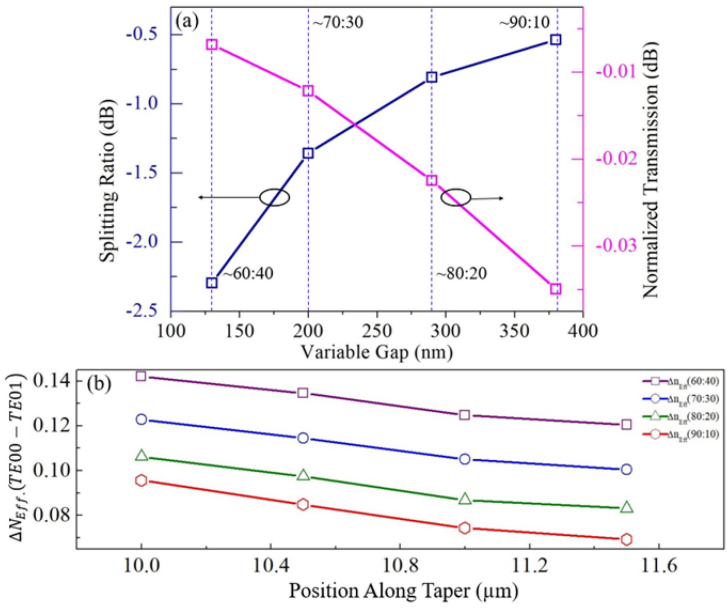

Fig. 5. (a) Different variable gaps corresponding to various arbitrary power splitting ratios and simulated insertion loss. (b). Difference in effective refractive index along the length of the taper; arbitrary power ratios of 60:40, 70:30, 80:20, and 90:10.

of greater than 230 nm (3.66–3.89 μm). Following the above design optimization, the taper length and tip width are selected to be 12 μm and 100 nm respectively. To demonstrate arbitrary splitting ratios, we select coupling gaps as shown in Table 1.

TABLE 1
Selected Coupling Gaps for Splitting Ratios of 50:50, 60:40 and 70:30

Gap (nm) (Fixed Coupling Gap, Variable Coupling Gap)	Splitting Ratios
100, 100 nm	50:50
100, 130 nm	60:40
100, 200 nm	70:30

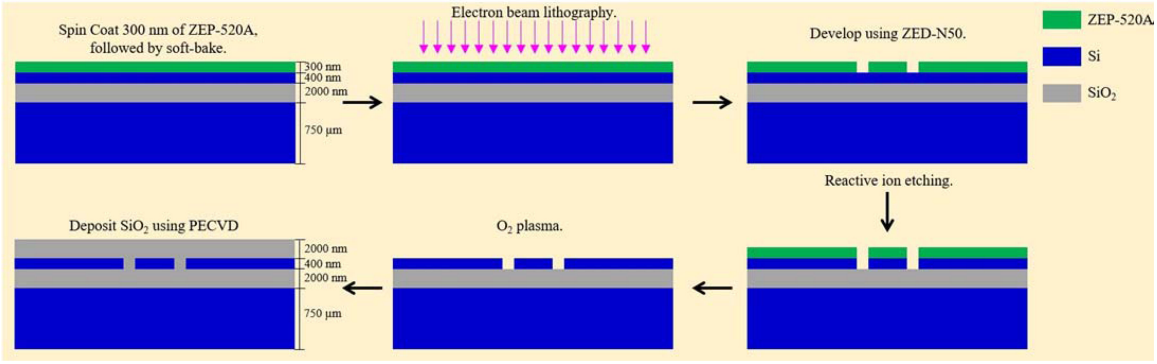

Fig. 6. Schematic process flow of the proposed power splitter.

3. Device Fabrication and Characterization

The fabrication process flow is shown in Fig. 6 . 300 nm of ZEP-520A is spin-coated followed by a soft-bake process on a 400 nm SOI platform. Electron Beam Lithography (EBL) was used to pattern the photoresist. Following, ZED-N50 was used to develop the sample. A single 400 nm etch step using Reactive Ion Etching (RIE) was then carried out to define the waveguides and the grating couplers. O_2 plasma etch was utilized to remove any remaining ZEP-520A. Finally, a 2 μm thick SiO_2 passivation layer is deposited using Plasma Enhanced Chemical Vapor Deposition (PECVD). The device footprint is estimated to be smaller than 12 $\times$ 2.9 μm^2. The power splitters are fabricated according to the optimized parameters obtained earlier. Arbitrary power splitters are fabricated according to the coupling gaps indicated in Table 1 (mentioned earlier). To demonstrate the consistency of the power splitting ratio, each power splitter is cascaded over 4 stages as shown in the micrograph image of Fig. 7(a). The insertion loss is obtained with the following approach.

$$IL\,(dB) = \frac{10\log_{10}\left(\frac{x_1+x_2+x_3+x_4+x_5}{x_0}\right)}{4} \tag{1}$$

Where $x_{1,2,3,4,5}$ corresponds to the power from each of the 5 outputs. x_0 refers to the output from the reference waveguide. A factor of 1/4 is used in consideration of the 4 stages. The insertion loss consists of splitter insertion loss and waveguide propagation loss. Grating coupler insertion loss is removed via (1) from the insertion loss characterization.

SEM images of the grating coupler, waveguide, arbitrary power splitter with coupling gaps of (100 nm, 100 nm) and (100 nm, 200 nm) are shown in Fig. 7(b)–7(d), respectively. The coupling gaps and taper lengths are measured to be consistent with the intended design parameters. However, the fabricated width of the tip width was found to be 45 nm. Nevertheless, according to

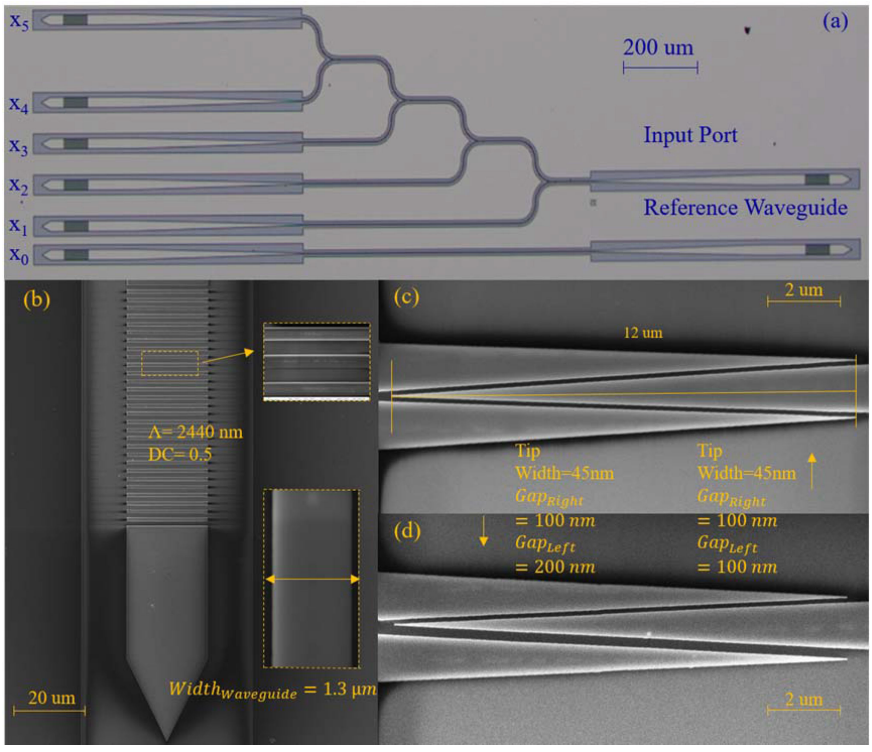

Fig. 7. (a) Micrograph image of 4 cascaded stages of power splitter. (b) SEM image of grating coupler and waveguide. (c) SEM image of coupling region with coupling gaps of 100, 100 nm. (d) SEM image of coupling region with coupling gaps of 100, 200 nm.

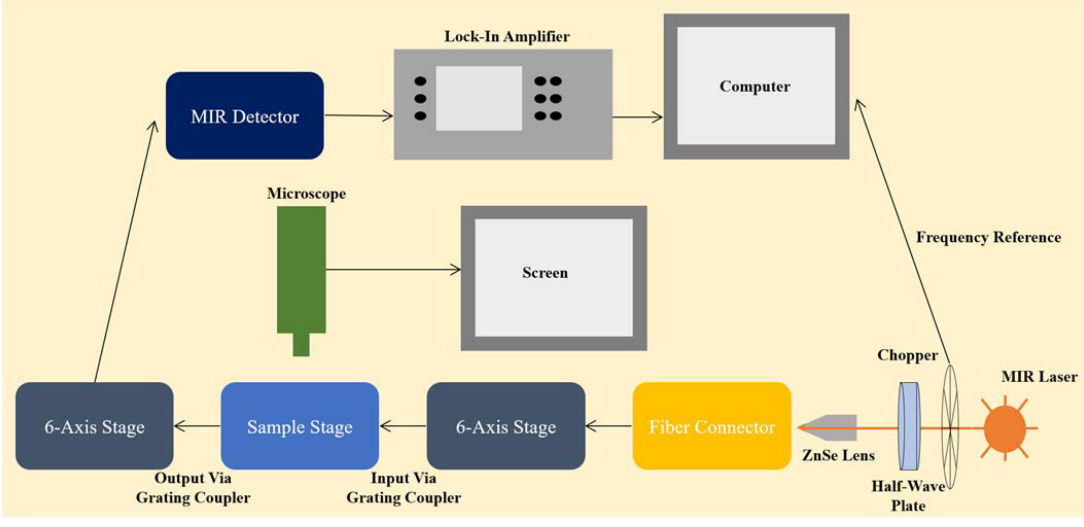

Fig. 8. Schematics of the experimental measurement set-up.

Fig. 3(b), the value of tip width has a large degree of fabrication tolerance from 30 to 120 nm. The measurement setup is shown in Fig. 8. The light source is a linearly polarized continuous wave tunable laser (Daylight Solution Inc, Model TLS-41038). A half wave plate (Altechna) is placed immediately after the chopper (Thorlabs MC2000) for fine polarization control. Light is launched

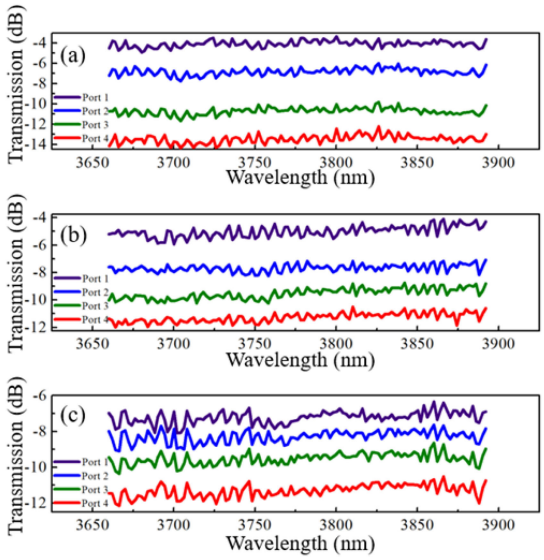

Fig. 9. Experimentally measured spectra at port 1, 2, 3 and 4 for power splitters with gap of (a) 100, (b) 130 and (c) 200 nm.

TABLE 2
Maximum and Minimum Levels of Insertion Loss for Arbitrary Power Splitters With Different Splitting Ratios

Gap (nm) (Fixed Coupling Gap, Variable Coupling Gap)	Splitting Ratio	IL_{min}(dB)	IL_{max}(dB)
100, 100	50:50	0.11	0.46
100, 130	60:40	0.14	0.48
100, 200	70:30	0.22	0.60

into the ZrF_4 mid-infrared fiber (FiberLabs) and focused via the ZnSe lens (INNOV). Light is then coupled into the device through grating couplers. The grating couplers used in this application have a period of 2440 nm, DC $=$ 0.5, and an etch depth of 400 nm. Light from the output grating coupler is then coupled to the fiber and directed towards the detector (Horiba DSS-IS020L), which is connected to the lock-in amplifier (AMETEK 7265).

Fig. 9(a)–(c) shows the experimentally measured spectra for devices with variable gaps of 100, 130, 200 nm respectively in the 4-stage testing structure (Fig. 7(a)). A wavelength sweep is performed from 3.66–3.89 μm and it is observed that the spectrum is relatively flat over the maximum tunable range of our laser. The minor fluctuations can be regarded as experimental noise as we can see that the specific line shape is present in each of the 4 ports. The broadband insertion loss for each beam splitter is shown in Fig. 10(a)–(c); the maximum and minimum values of device insertion loss is indicated in Table 2.

For accurate characterization of the splitting ratios, 4-stage and single stage testing structures are utilized. Firstly, for the 4-stage testing structure (Fig. 7(a)), the measured output power at each port was linearly fitted at 3.8 μm. According to Fig. 11(a)–(c), we have managed to obtain splitting

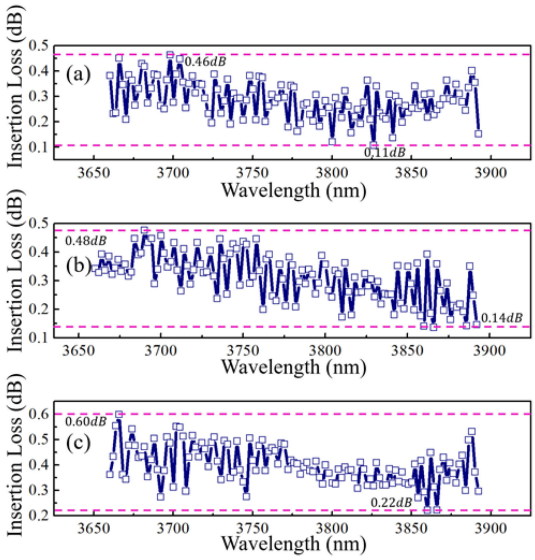

Fig. 10. Experimentally measured device broadband insertion loss (3.66–3.89 μm) with gaps of (a) 100, (b) 130 and (c) 200 nm.

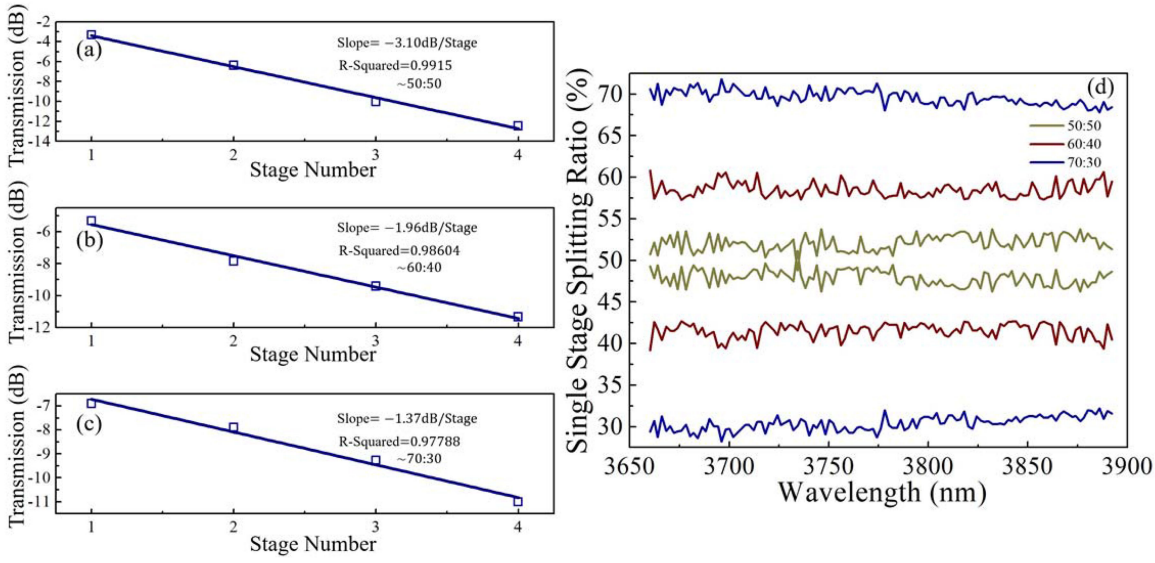

Fig. 11. (a)–(c) Linear fit for power splitters with gap of 100, 130, 200 nm across 4 output ports. (d) Splitting ratios of the single-stage power splitter.

ratios of −3.10 dB (∼50:50), −1.96 dB (∼60:40) and −1.37 dB (∼70:30) for power splitters with variable gaps of 100, 130 and 200 nm respectively. The ratios between the 2 output ports (Fig. 1) of the single-stage testing structures across 3.66–3.89 μm are indicated in Fig. 11(d). The splitting ratios obtained from the single-stage testing structures validates the results from Fig. 11(a)–(c). The coupling gaps fabricated to obtain splitting ratios of 50:50, 60:40 and 70:30 are shown to agree closely with the simulated results in Fig. 5(a). Table 3 provides a brief comparison of this work with some arbitrary power splitters in the literature.

TABLE 3
Overview of Some Arbitrary Power Splitters in Literature

Mechanism	Wavelength	Insertion Loss	Splitting Ratios Obtained	Bandwidth
Asymmetric MMI [23]	~1.55 μm	~0.3 dB	50:50, 60:40, 70:30, 80:20, 90:10	60 nm
"QR" Code MMI [24]	~1.55 μm	~1.0 dB	50:50, 67:33, 75:25	30 nm
Angled Sub-Wavelength Grating MMI [25]	~1.55 μm	Not Stated	50:50, 60:40, 80:20, 90:10	100 nm
Rib Waveguide Dispersion DC [26]	~3.8 μm	~0.6 dB	50:50* 100:0	85 nm* 230 nm
Asymmetric-Waveguide based phase control [27]	~1.55 μm	<1 dB	50:50, 60:40, 70:30, 80:20, 90:10	75-100 nm
Presented Work	***~3.8 μm***	***0.11-0.6 dB***	***50:50, 60:40, 70:30***	***230 nm***

4. Conclusions

In conclusion, through the design and optimization of anti-symmetrical adiabatic evolution-based power splitters, we have experimentally demonstrated splitting ratios of 50:50, 60:40 and 70:30. Broadband operation and low broadband insertion loss have been obtained from 3.66–3.89 μm (230 nm). The tip width, being the smallest feature in the device, has a large degree of fabrication tolerance, paving the possibility for this device to be fabricated in commercial CMOS process lines. The fabrication of the device is simple, only requiring a single etch step. Broadband operation (230 nm), low broadband insertion loss (0.11–0.6 dB), CMOS compatibility, compact footprint and ease of fabrication makes this device a strong candidate to serve as a fundamental component in commercial scale MIR integrated optics.

References

[1] B. Troia *et al.*, "Design procedure and fabrication of reproducible silicon Vernier devices for high-performance refractive index sensing," *Sensors*, vol. 15, no. 6, pp. 13548–13567, 2015.
[2] X. Xu, C. Chung, Z. Pan, H. Yan, and R. T. Chen, "Periodic waveguide structures for on-chip modulation and sensing," *Jpn. J. Appl. Phys.*, vol. 57, no. 8S2, 2018, Art. no. 08PA04.
[3] A. D. Ellis, N. Mac Suibhne, D. Saad, and D. N. Payne, "Communication networks beyond the capacity crunch," *Philos. Trans. Roy. Soc. A*, vol. 374, no. 2062, 2015, Art. no. 20150191.
[4] Z. Li, A. M. Heidt, J. M. O. Daniel, Y. Yung, S. U. Alam, and D. J. Richardson, "Thulium-doped fiber amplifier for optical communications at 2 μm," *Opt. Exp.*, vol. 21, no. 8, pp. 9289–9297, 2013.
[5] R. Soref, "Mid-infrared photonics in silicon and germanium," *Nature Photon.*, vol. 4, pp. 495–497, 2010.
[6] V. M. Lavchiev and B. Jakoby, "Photonics in the mid-infrared: Challenges in single-chip integration and absorption sensing," *IEEE J. Sel. Topics Quant. Electron.*, vol. 23, no. 2, Mar./Apr. 2017, Art. no. 8200612.
[7] B. Dong *et al.*, "Silicon-on-insulator waveguide devices for broadband mid-infrared photonics," *Photon. J.*, vol. 9, no. 3, 2017, Art. no. 4501410.

[8] T. Hu *et al.*, "Silicon photonic platforms for mid-infrared applications [Invited]," *Photon. Res.*, vol. 5, no. 5, pp. 417–430, 2017.
[9] R. Shankar and M. Loncar, "Silicon photonic devices for mid-infrared applications," *Nanophotonics*, vol. 3, no. 4–5, pp. 329–341, 2014.
[10] E. D. Palik, *Handbook of Optical Constants of Solids (Academic, 1998)*, vol. 1. London, U.K.: Elsevier, 1998, ch. 11, pp. 213–270.
[11] L. He *et al.*, "Loss reduction of silicon-on-insulator waveguides for deep mid-infrared applications," *Opt. Lett.*, vol. 42, no. 17, pp. 3454–3457, 2017.
[12] R. Wang, A. Malik, I. Simontye, A. Vizbaras, and G. Roelkens, "Compact GaSb/silicon-on-insulator 2.0x μm widely tunable external cavity lasers," *Opt. Exp.*, vol. 24, no. 25, pp. 28977–28986, 2016.
[13] R. Wang *et al.*, "Widely tunable 2.3 μm III-V-on-silicon Vernier lasers for broadband spectroscopic sensing," *Photon. Res.*, vol. 6, no. 9, pp. 858–866, 2018.
[14] W. Wang *et al.*, "Mid-infrared (MIR) Mach–Zehnder silicon modulator at 2 μm wavelength based on interleaved PN junction," in *Proc. Conf. Lasers Electro-Opt.* , 2018, paper STh1B.1.
[15] W. Cao *et al.*, "High-speed silicon modulator for the 2 μm wavelength band," *Optica*, vol. 5, no. 9, pp. 1055–1062, 2018.
[16] J. J. Ackert *et al.*, "High-speed detection at two micrometers with monolithic silicon photodiodes," *Nature Photon.*, vol. 9, pp. 393–396, 2015.
[17] W. Zhou, Z. Cheng, X. Wu, B. Zhu, X. Sun, and H. K. Tsang, "Fully suspended slot waveguide for high refractive index sensitivity," *Opt. Lett.*, vol. 42, no. 7, pp. 1245–1248, 2017.
[18] H. Lin *et al.*, "Mid-infrared integrated photonics on silicon: A perspective," *Nanophotonics*, vol. 7, no. 2, pp. 393–420, 2018.
[19] A. Spott, E. J. Stanton, N. Volet, J. D. Peters, J. R. Meyer, and J. E. Bowers, "Heterogeneous integration for mid-infrared silicon photonics," *IEEE J. Sel. Topics Quant. Electron.*, vol. 23, no. 6, Nov./Dec. 2017, Art. no. 8200810.
[20] Y. Zou, S. Chakravarty, C. Chung, X. Xu, and R. T. Chen, "Mid-infrared silicon photonic waveguides and devices [Invited]," *Photon. Res.*, vol. 6, no. 4, pp. 254–276, 2018.
[21] C. Zhao, C. Peng, and W. W. Hu, "Blueprint for large-scale silicon optical phased array using electro-optical micro-ring pixels," *Sci. Rep.*, vol. 7, no. 1, pp. 1–12, 2017.
[22] A. Zanzi, A. Brimont, A. Griol, P. Sanchis, and J. Marti, "Compact and low-loss asymmetrical multimode interference splitter for power monitoring applications," *Opt. Lett.*, vol. 41, no. 2, pp. 227–229, 2016.
[23] Q. Deng, L. Liu, X. Li, and Z. P. Zhou, "Arbitrary-ratio 1 $\times$ 2 power splitter based on asymmetric multimode interference," *Opt. Lett.*, vol. 39, no. 19, pp. 5590–5593, 2014.
[24] K. Xu *et al.*, "Integrated photonic power divider with arbitrary power ratios," *Opt. Lett.*, vol. 42, no. 4, pp. 855–858, 2017.
[25] E. El-Filky *et al.*, "Ultra-broadband and compact asymmetrical beam splitter enabled by angled subwavelength grating MMI," in *Proc. Conf. Lasers Electro-Opt.*, 2018, paper STh4A.7.
[26] B. Dong *et al.*, "Compact low loss mid-infrared wavelength-flattened directional coupler (WFDC) for arbitrary power splitting ratio enabled by rib waveguide dispersion engineering," *IEEE J. Sel. Topics Quant. Electron.*, vol. 24, no. 4, Jul./Aug. 2018, Art. no. 4500108.
[27] Z. Lu *et al.*, "Broadband silicon photonic directional coupler using asymmetric-waveguide based phase control," *Opt. Exp.*, vol. 23, no. 3, pp. 3795–3808, 2015.
[28] Y. Wang, S. Gao, K. Wang, and E. Skafidas, "Ultra-broadband and low-loss 3 dB power splitter based on adiabatic silicon waveguides," *Opt. Lett.*, vol. 41, no. 9, pp. 2053–2056, 2016.
[29] J. Xiao and Z. Guo, "Ultracompact polarization-insensitive power splitting using subwavelength gratings," *Photon. Technol. Lett.*, vol. 30, no. 6, pp. 4220–4223, 2013.
[30] X. Li, H. Xu, X. Xiao, Z. Li, J. Yu, and Y. Yu, "Compact and low-loss silicon power splitter based on inverse tapers," *Opt. Lett.*, vol. 38, no. 20, pp. 4220–4223, 2013.